JOURNAL OF AIRCRAFT
Vol. 39, No. 6, November–December 2002

Aspects of Flow Transition Detection When Flight Testing Engine Nacelles

Hansgeorg Riedel* and Martin Sitzmann*
DLR, German Aerospace Research Center, D-38108 Brunswick, Germany

Some lessons learned as regards flow transition detection in the course of flight-testing carbon fiber composite conventional and laminar flow nacelles are presented. The key objective of the flight trials was to examine the influences of environmental phenomena and of the engine nacelle structure regarding the interpretation of the nacelle infrared images and of the nacelle surface temperature measurements, both with reference to determining the location of the flow transition front on the nacelles. As regards the application of the infrared thermography, the study has yielded the result that the quality of the infrared images is influenced by heat radiation to space and from the Earth, as well as by reflection of sunlight from the airframe. For good quality infrared images, only carbon fiber composites should be used as structural material for the nacelle fan cowls. In addition, the mechanical design of the fan cowls should not contain any stiffening frames in the substructure, but they should be designed as a uniform honeycomb skin structure. Concerning the surface temperature measurements, for good-quality results, a uniform honeycomb carbon fiber composite skin structure is just as essential as for the infrared imaging system.

Nomenclature

C_P	=	static pressure coefficient, $(p - p_\infty)/\frac{1}{2}\rho_\infty U_\infty^2$
c	=	fan cowl chord, 1050 mm for Datum nacelle and 1035.8 mm for natural laminar flow and hybrid laminar flow nacelles
d	=	thickness
H	=	altitude
M_∞	=	freestream Mach number
N_{1C}	=	corrected engine speed; corrected low-pressure rotating assembly speed
p	=	static pressure
Re_c	=	Reynolds number based on fan cowl chord
$T_{t\infty}$	=	freestream total temperature
T_W	=	surface (wall) temperature
t	=	time
U_∞	=	freestream velocity
x	=	axial coordinate measured from fan cowl highlight plane (Fig. 5)
α	=	angle of incidence referred to fuselage axis
β	=	angle of yaw
ρ	=	density
φ	=	circumferential angle (radial) (Fig. 10)

Subscripts

c	=	fan cowl chord
L	=	laminar
T	=	turbulent
Tfo	=	fully turbulent flow onset
Tr	=	transition
Tro	=	transition onset
W	=	wall (surface)
∞	=	freestream

Received 19 April 2001; revision received 20 May 2002; accepted for publication 20 May 2002.

*Research Scientist, Institut für Aerodynamik und Strömungstechnik, Department Transportflugzeuge, Lilienthalplatz 7.

Introduction

BY the application of laminar flow technology in aeronautics, substantial improvements in the areas of economy and ecology can be achieved with reference to aircraft operation. A prerequisite for a successful application of the laminar flow technology are complementary approaches using numerical and experimental tools. As for the experimental tools, by conducting flight trials this procedure has two advantages. First, the results obtained relate to a realistic environment and not to simulated conditions, as encountered, for instance, when performing tests in wind tunnels. Second, the Reynolds numbers associated with the flight testing represent realistic values.

In regard to the laminarization of engine nacelles, as for any other aircraft surfaces such as wing or fin, there are in principle three laminar flow concepts available.[1–5]

1) The concept of natural laminar flow control (NLFC) depends solely on shaping the surface under consideration to produce a favorable pressure gradient, that is, at high Reynolds numbers accelerated flow, over as much of the surface as is physically possible to maintain laminar flow. This concept has, however, the basic disadvantage that for a nacelle the maximum nacelle diameter is increased compared with a conventional nacelle. Consequently the achievable maximum cruise Mach number is reduced because, in the case of current subsonic transport aircraft, the maximum extent of laminar flow is in general shock limited.

2) In the concept of laminar flow control (LFC) by suction, the boundary layer on the surface is kept in a laminar flow state by applying distributed suction. Based on structural considerations, the most efficient way of employing suction is by sucking through a microperforated surface instead of stripwise sucking through slots.

3) The concept of hybrid laminar flow control (HLFC) combines the NLFC and the LFC concepts. It implies that, in the case of an engine nacelle, the aerodynamic shape some short distance downstream of the nacelle leading edge allows a short region of adverse static pressure gradient to be established in which suction is applied to maintain laminar flow. The extent of the suction region is typically 10–25% of the nacelle fan cowl chord. The suction region is followed by a more extensive unsucked region incorporating a favorable pressure gradient as result of suitably shaping the nacelle fan cowl. The HLFC concept leads to a much slimmer nacelle fan cowl contour compared with an NLF nacelle, the maximum nacelle diameter being significantly reduced. The result is a lower peak Mach number on the nacelle, yielding a higher maximum cruise Mach number. Figure 1 illustrates the basic differences of the fan cowl geometry associated with an NLF and an HLF nacelle in comparison with a conventional nacelle. Also schematically shown are representative

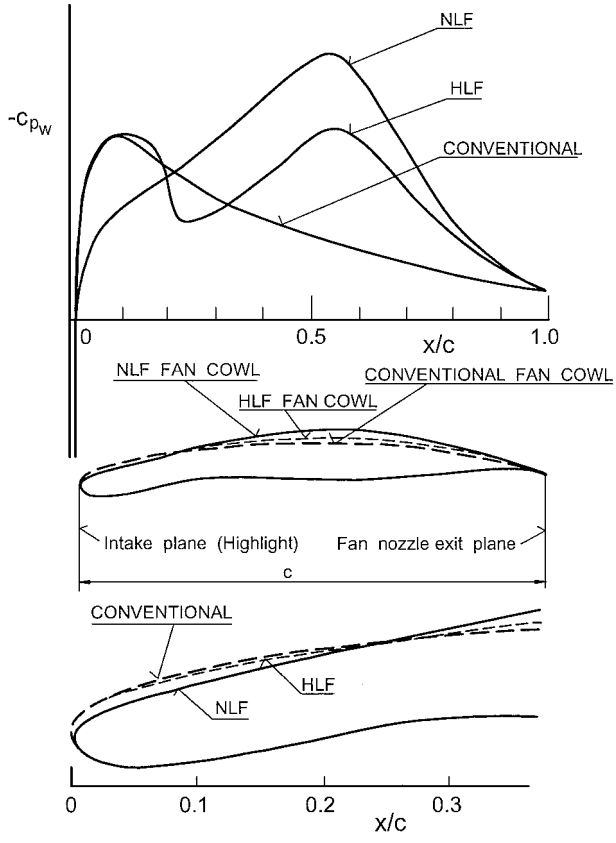

Fig. 1 Typical conventional, NLF, and HLF nacelle fan cowl geometries and schematic of the associated external fan cowl surface static pressure distributions.

distributions of the surface static pressure coefficients C_{PW} on the fan cowl corresponding to each of the nacelles addressed.

The present paper deals with some observations made and lessons learned concerning the flow transition detection in the course of flight testing carbon fiber composite conventional and laminar flow nacelles, the latter constituting an NLF and an HLF nacelle. Particular aspects covered are the influences of environmental phenomena and of the engine nacelle structure with reference to the interpretation of the infrared images and of the surface temperature measurements for the respective nacelle fan cowls. For both flow transition detection techniques, the primary goal is the determination of the location of the transition front. The term front here does not refer to a definite line separating the laminar from the turbulent flow. On the contrary, in agreement with the physical nature of the flow, it defines the locus of the midpoints of the boundary-layer region in which the flow changes from the fully laminar to the fully turbulent state in the streamwise direction.

The results addressed were obtained during flight trials conducted within the framework of a European collaborative program using the German Aerospace Research Center (DLR) flight-test aircraft Vereinigte Flugtechnische Werke VFW614/Advanced Technologies Testing Aircraft (ATTAS) as flight-test vehicle. In a first series of flight tests during September/October 1992, the NLF nacelle was installed on the VFW614/ATTAS. A second flight-test series performed with this nacelle followed in April/May 1993, during which also a Datum nacelle possessing a conventional geometry was flight tested for comparison with the NLF nacelle.[1,2] The flight test program was later extended to flight test an HLF nacelle featuring boundary-layer suction and insect contamination protection.[2] The flight tests with the HLF nacelle were performed in a third flight-test series during September/October 1993.

Flight-Test Vehicle and Nacelles

Flight-Test Vehicle

The DLR flight test aircraft VFW614/ATTAS is a modification of the basic VFW614 and was originally intended by DLR to be operated primarily for developing and evaluating advanced technologies in the areas of flight mechanics, as well as flight control and guidance. However, with the growing interest in the application of the laminar flow technology, this test vehicle has also recently been used for aerodynamic investigations on laminar flow over wings[6] and engine nacelles.[1–5] Further details of the flight-test vehicle are contained in Ref. 4. Figure 2 shows the VFW614/ATTAS in side and plan view, and Fig. 3 shows a partial view of the flight-test vehicle in flight with the NLF nacelle installed on the port engine, while the starboard engine features the production standard nacelle.

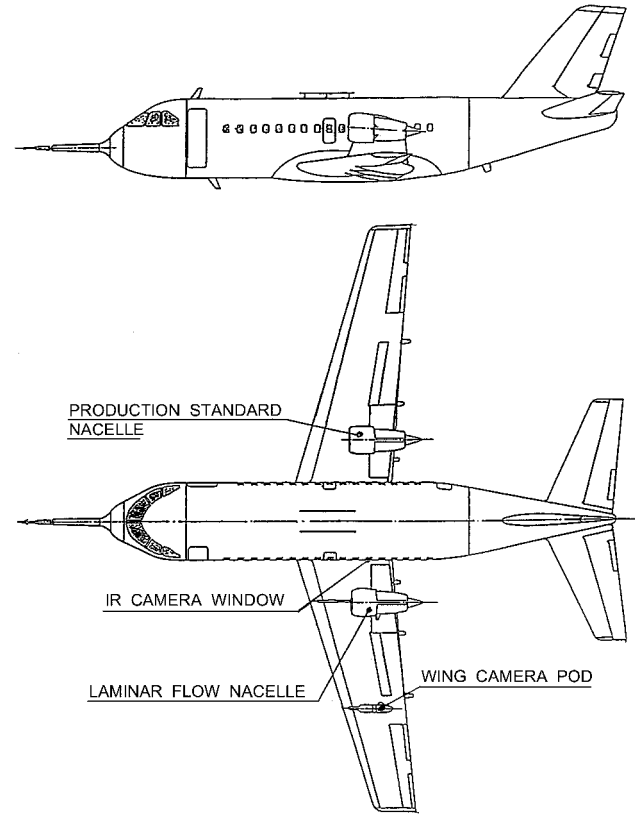

Fig. 2 VFW614/ATTAS with laminar flow nacelle installed on the port engine.

Fig. 3 VFW614/ATTAS in-flight with the NLF nacelle installed on the port engine.

Flight-Test Nacelles

The aircraft configuration for flight testing the different flight-test nacelles, the Datum, the NLF and the HLF nacelles, entailed that, for the port engine the fan cowl of the conventional, that is, production standard, nacelle, which is completely metal, was replaced by the respective flight-test fan cowls. These were fabricated using carbon fiber composite (CFC). In this context, note that, when referring to the Datum nacelle, the NLF nacelle or the HLF nacelle for that matter, this relates only to the fan cowl of the particular nacelle because, for the flight trials, in all cases the metal core cowl and the plug of the engine remained unaltered.[4]

To avoid having to build a complete HLF nacelle, the solution adopted was to modify the existing NLF nacelle outboard fan cowl by fitting an HLF panel insert (glove) at an appropriate circumferential position, so that all characteristic features of an HLF nacelle were obtained. With reference to Fig. 4, the HLF panel insert consists of a wash zone at the leading edge of the fan cowl and an adjacent suction zone. The wash zone is part of a liquid transpiration insect anticontamination system and, in the suction zone, suction is applied through the microperforated fan cowl surface to prevent transition of the boundary-layer flow from the laminar to the turbulent state. The resulting geometry of the HLF nacelle fan cowl differed from that shown in Fig. 1, describing the characteristic geometric features of an HLF nacelle fan cowl in comparison with the fan cowls of an NLF and a conventional nacelle. The main difference of the HLF nacelle designed for the VFW614/ATTAS is that the maximum diameter of the HLF nacelle fan cowl is the same as for the NLF nacelle fan cowl. Figure 5 shows a comparison of the fan cowl geometries for the Datum, the NLF, and the HLF nacelles that were flight tested on the VFW614/ATTAS. As regards the distributions of the surface static pressure coefficients C_{PW} on the fan cowls, also schematically shown in Fig. 5 for the variety of nacelles tested, the rear suction peak associated with the HLF nacelle fan cowl (at $x/c \sim 0.5$) reaches the same level as the suction peak of the NLF nacelle fan cowl. This is in contrast to the situation shown in Fig. 1, which corresponds to a design free of any constraints and which represents the ideal case.

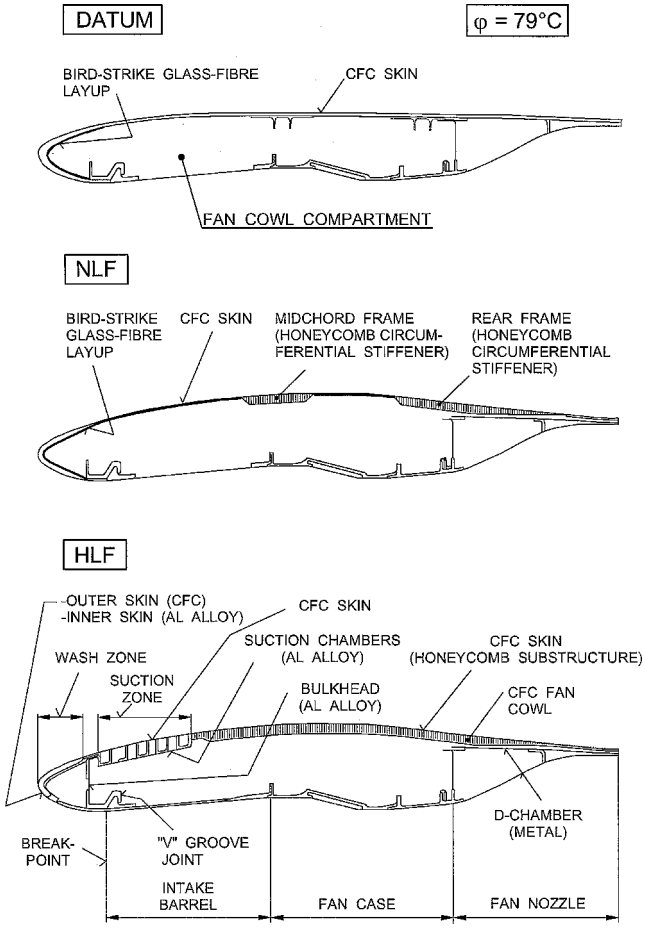

Fig. 4 Details of the fan cowl structure of the Datum, NLF, and HLF nacelles at $\varphi = 79$ deg.

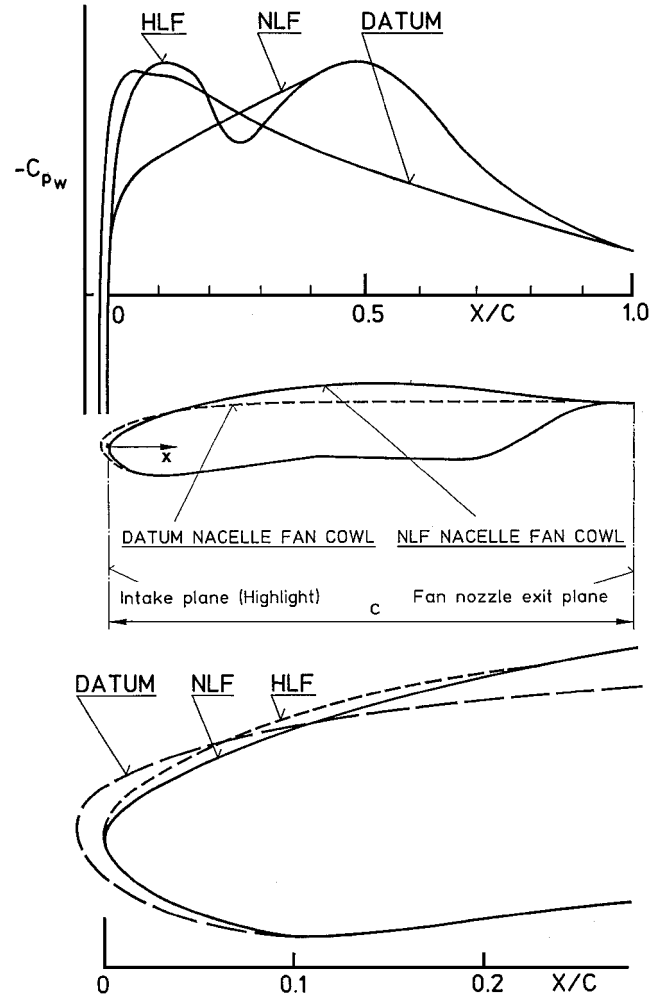

Fig. 5 Comparison of the Datum, NLF and HLF fan cowl geometries of the respective nacelles flight tested on the VFW614/ATTAS and schematic of the associated external fan cowl surface static pressure distributions.

Infrared Thermography

Infrared Imaging System

For the global transition detection on the fan cowls of the flight-test nacelles of the VFW614/ATTAS use was made of the infrared thermographic technique. A comprehensive survey of the application of the infrared thermography in aerodynamic research is contained in Ref. 7. Physical aspects of the infrared thermography and details of some subsonic studies in wind tunnels and free flight to investigate transition patterns on wings employing infrared imaging are described in Ref. 8.

An overview of the infrared camera locations on the VFW614/ATTAS is shown in Fig. 2. The outboard fan cowl thermograms were gained with the aid of an infrared camera mounted inside a wing camera pod. The inboard fan cowl thermograms were obtained with an infrared camera placed in one of the fuselage (cabin) windows.

Influence of Environmental Phenomena

The infrared thermography utilizes the physical flow property that different rates of heat transfer exist for the boundary-layer flow over the target surface (fan cowl), depending on whether the boundary-layer flow is laminar or turbulent. Correspondingly, different surface temperature levels will be established in those two flow regions.

Table 1 VFW614/ATTAS flight conditions associated with various test points

	First test series	Second test series		Third test series	
Nacelle	NLF	DATUM	NLF	HLF	HLF
Test point	306	412	621	821	823
Flight	19	24	32	39	39
Date	1 Oct. 1992	16 April 1993	4 May 1993	20 Sept. 1993	20 Sept. 1993
Time	1027:54	1126:3.60	0832:16.48	1111:34.64	1119:46.35
M_∞	0.56	0.45	0.56	0.50	0.45
H, m	6,521	6,486	6,459	6,435	6,471
α, deg	1.8	3.6	1.4	2.3	3.4
β, deg	0.1	−0.2	−0.1	0.3	−0.1
Re_c	7.1×10^6	6.1×10^6	7.5×10^6	6.3×10^6	5.6×10^6
N_{1c}, %	95.0	86.5	97.7	93.3	93.7
dH/dt, m/s	0.05	0.53	0.72	0.10	0.14

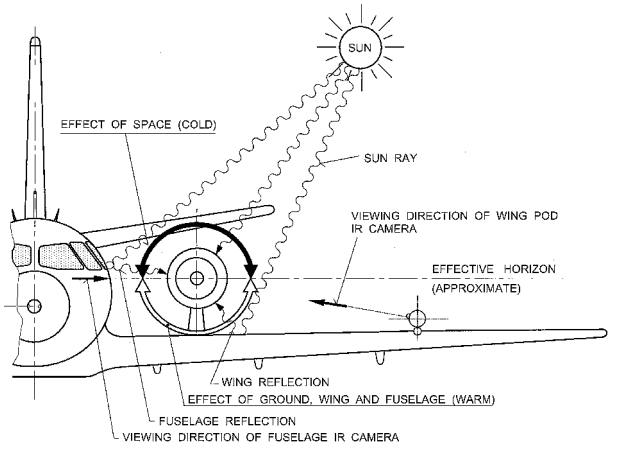

Fig. 6 Schematic highlighting environmental phenomena affecting the infrared images of the nacelle.

For the flight trials of the flight-test nacelles, the goal was in general to operate the flight-test vehicle under conditions allowing the surface temperature of the fan cowl to be higher than the freestream temperature. With the normal operating mode of the infrared imaging system and proper settings of brightness and contrast, on the thermogram the region with laminar boundary-layer flow will be identifiable by a lighter shaded area in contrast to the region of turbulent boundary-layer flow that will be featuring a darker shaded area.

For the application of the infrared thermographic technique in flight testing, the influence of the environment plays an important role. Figure 6 shows some major effects associated with environmental phenomena for the flight trials with the VFW614/ATTAS. First, there is the effect of space. The space as background is at a low temperature, which is definitely lower than the temperature on any aircraft surface, and this will lead to heat radiation from the aircraft surfaces exposed to space, resulting in a reduction of the temperature of those surfaces. Second, there exists the effect of the ground (surface of the Earth). The surface temperature of the Earth is in general higher than the temperature of most aircraft surfaces for typical cruise altitudes $H > 20{,}000$ ft and for subsonic flight Mach numbers, excluding the visible core nozzle exit and the plug of the engine. Thus, components of the aircraft exposed to heat radiation from the ground will experience a temperature rise. For the fan cowl of the engine nacelle on the VFW614/ATTAS, both of the mentioned environmental influences result in a division of the fan cowl into an upper half, which is subjected to heat radiation into space with an associated temperature reduction, and a lower half, which is receiving heat radiation from the ground leading to a temperature rise (Fig. 6). Third, superimposed on the influences of the space and the ground is the effect of the heat radiation from the sun. This causes a heating of the aircraft surfaces exposed to sun rays. Certain fan cowl areas not exposed to the direct sunlight can be subjected to heat radiation of the sun that is reflected, for example, from the wing or the fuselage (Fig. 6), thus raising the surface temperature in those areas accordingly.

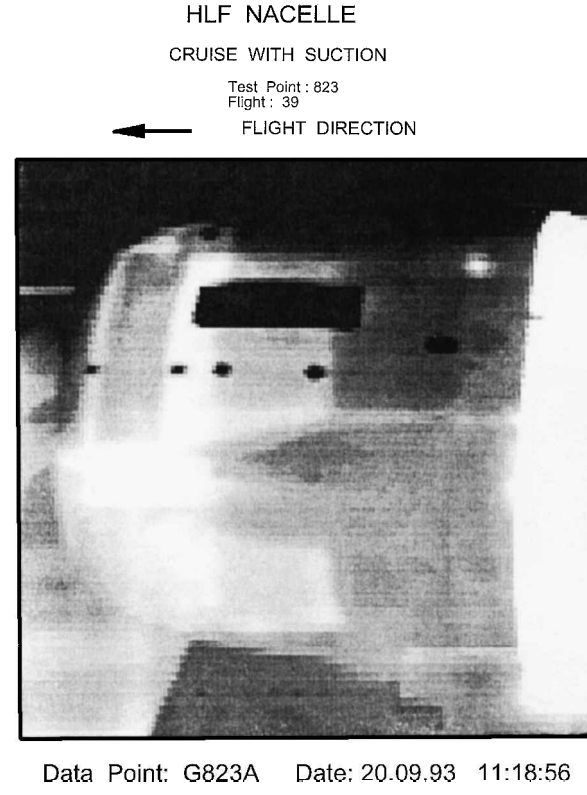

Fig. 7 Typical infrared image of the outboard side of the HLF nacelle fan cowl, illustrating the influence of environmental phenomena and fan cowl structural features (cruise condition with suction, TP 823).

A typical example of a thermogram is shown in Fig. 7, which features the outboard fan cowl of the HLF nacelle at cruise (test point 823). Details of the associated flight conditions are listed in Table 1. The schematic of Fig. 8 serves to elucidate various aspects of information contained in the thermogram. The main features observed in connection with the thermogram and the schematic of Fig. 8 are the following, noting that warmer surface regions of the fan cowl correspond to lighter shaded areas and colder surface regions appear darker. The run of laminar boundary-layer flow on the fan cowl (area of lighter shade) extends to $x/c = 0.60$, excluding some embedded turbulent wedges. The turbulent boundary layer on the fan cowl (darker shaded area) covers the fan cowl from $x/c = 0.60$ to the fan cowl nozzle exit, including the turbulent wedges addressed. The fan flow appears as white area because, dependent on the engine speed, the total temperature in the fan flow exceeds the total temperature of the freestream by 30–40°C and is, thus, considerably higher than the temperature of any other object within the frame of the infrared image. The lower half of the fan cowl features a lighter shaded region than the top half as result of the heat radiation received from the sun rays reflected on the wing. In side view, the fan cowl is not a plane surface but approximates to the convex surface of a circular

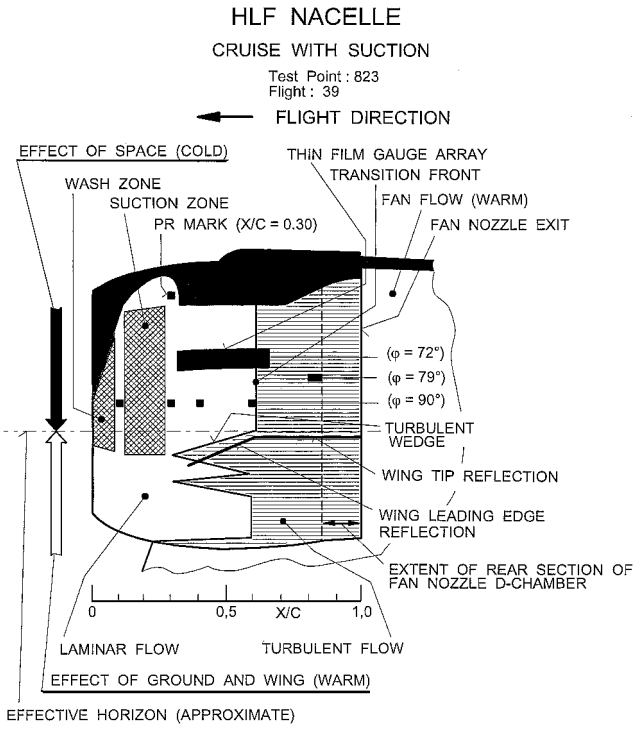

Fig. 8 Schematic of the infrared image for the outboard side of the HLF nacelle fan cowl, illustrating the influence of environmental phenomena and fan cowl structural features (cruise condition with suction, TP 823).

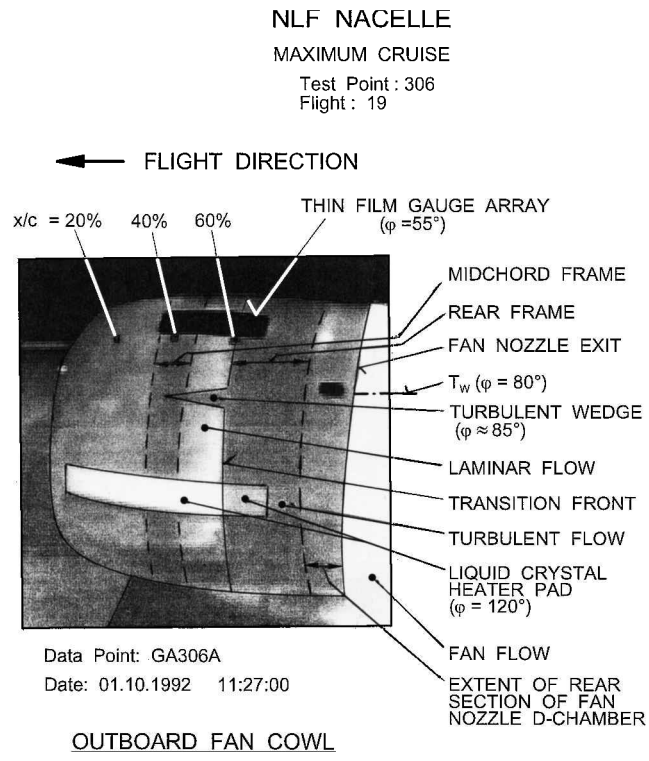

Fig. 9 Infrared image of the outboard fan cowl of the NLF nacelle for the condition of maximum cruise (TP 306), showing the effect of environmental phenomena and of the fan cowl structural features.

cylinder with its axis horizontal. The heat radiation received by the wing pod infrared camera (Fig. 6) along the outer edges of the camera viewing angle, corresponding to the vicinity of the crown and of the keel on the fan cowl, respectively, is very low. Because of the radiation properties of nonmetallic surfaces,[9] the heat radiation intensity drops rapidly to zero as a tangential viewing direction to the surface is approached from the normal direction. Consequently, although at the crown and at the keel the surface temperature is not significantly different from that of other parts on the fan cowl, the infrared camera system interprets the lower radiation intensity received as a reduced temperature so that those areas near the crown and keel appear as darker shaded regions on the thermogram than the rest of the fan cowl. This surface curvature effect, making itself felt as an apparent surface temperature reduction, is also evident from the wing tip reflection and wing leading-edge reflection superimposed on the infrared image of the upper turbulent wedge in Fig. 7.

Influence of Engine Nacelle Structure and Instrumentation

The influence of the engine nacelle structure on the fan cowl surface temperature distribution makes itself felt in several ways. As already addressed, the operation of the fan will cause a total temperature rise of 30–40°C in the fan flow downstream of the fan relative to the freestream total temperature depending on the engine speed. This means (cf. Fig. 4) that the section of the fan case downstream of the location of the fan and the fan nozzle will experience a temperature increase as result of the heat transfer from the fan flow. By heat conduction, heat will spread via the fan case to the intake barrel. The CFC fan cowl and the intake barrel–fan case–fan nozzle assembly enclose a confined space, the fan cowl compartment. By heat transfer from the intake barrel–fan case–fan nozzle assembly into the fan cowl compartment, the air contained in this compartment will in general also heat up to a certain extent. There is some ventilation of the fan cowl compartment. As result, in the fan cowl compartment, a longitudinal temperature gradient will build up reaching the highest temperature near the fan cowl trailing edge. Although the CFC structure of the fan cowl is a poor heat conductor, heat will eventually be conducted from the fan cowl internal surface to the external surface of the fan cowl. Evidence for this is shown, for example, in the thermogram of Fig. 7 for the HLF nacelle fan cowl, where, in the region of the rear section of the fan nozzle D-chamber, the light shade is indicative of a higher surface temperature compared with the conditions in the region upstream and which is limited by the transition front. Figure 7, however, also reveals other substructure effects for the HLF nacelle fan cowl. Both the inner skin of the wash zone and the suction chambers are made of aluminium alloy, while their external surfaces are covered by the CFC skin (Fig. 4). Because the heat capacity of both those aluminium structures is large relative to that of the CFC skin covering, a local cooling effect on the CFC fan cowl skin is exerted by the aluminium alloy. This is because this material adjusts itself more rapidly to the near ambient temperature conditions prevailing in the front section of the fan cowl compartment because of the ventilation of this compartment. Although the wash zone and the suction zone lie within the laminar flow region of the fan cowl, they are visible on the infrared images as darker shaded areas compared with their surroundings because of the associated lower temperature.

As regards the NLF nacelle fan cowl, Fig. 9 shows the thermogram of the outboard fan cowl for the condition of maximum cruise [test point (TP) 306]. Details associated with this flight condition are shown in Table 1. Infrared images for the condition of maximum cruise have been discussed in Ref. 4, which is focused on the effect of the fan cowl structure with respect to differing heat properties. With the aid of Fig. 4, it is possible to identify in Fig. 9 those structural elements of the CFC fan cowl that are prominent as regards their heat properties. Thus, both the midchord frame ($0.35 < x/c < 0.45$) and the rear frame ($0.60 < x/c < 1.00$) appear on the thermogram as darker shaded areas compared with their surroundings because of their lower temperature levels that are associated with the larger heat capacity of the frames relative to the comparatively thin CFC skin adjacent to them.

With regard to the influence of the instrumentation, prominently visible on the thermograms are the thin-film gauge arrays, whereas the liquid crystal heater pads are only faintly discernable, provided the electric heaters of the pads are not in operation. The thin-film gauge arrays act like mirrors to the heat radiation from the sun, and

thus, they appear on the thermograms as black areas because of their low surface temperatures (cf. Figs. 7 and 9).

Fan Cowl Surface Temperature Measurements

Surface Temperature Sensors

Surface temperature measurements on aerodynamic surfaces can be helpful in detecting the location of the transition front on such surfaces. They are of particular value for those regions of the aerodynamic surfaces of interest that lie outside the field of view of infrared imaging systems, if these are employed to obtain a global view of the location of the transition front. For the surface temperature measurements on the fan cowls of the flight-test nacelles, use was made of platinum resistance thermometers as sensors.

Results and Analysis

Typical examples of the surface temperature distribution on the NLF nacelle fan cowl at radials $\varphi = 80$ and 285 deg, respectively, obtained in the first flight-test series, are illustrated for TP 306 in Fig. 10 for maximum cruise condition. Contrary to expectation, the surface temperature distributions do not display the expected trend of a higher temperature level in the region of laminar flow in comparison with the temperature level in the turbulent flow region. In fact, when use is made of the results obtained with the infrared thermography (cf. Fig. 9), for $\varphi = 80$ deg the transition front should lie at $x/c = 0.60$. In contrast, TP 306 in Fig. 10 shows that the measurements exhibit definite temperature peaks at the positions of the fan cowl stiffeners, that is, the bird-strike glass-fiber layup, the midchord frame, and the rear frame. It appears that at these components of the CFC fan cowl substructure the temperature sensors were not placed directly underneath the paint layer on the fan cowl external surface as specified, thus measuring in effect higher temperatures corresponding to those prevailing in the fan cowl compartment.

To remedy this situation, for the second flight-test series with the NLF nacelle, the temperature sensors were required to be relocated to comply with the specification. This was done, and the result for the temperature distribution at $\varphi = 80$ and 285 deg is shown in Fig. 11 for TP 621, which also is for the maximum cruise condition. Details of the flight conditions compared with those of TP 306 are given in Table 1. The temperature distributions for TP 621 are no longer found to exhibit the temperature peaks observed in the case

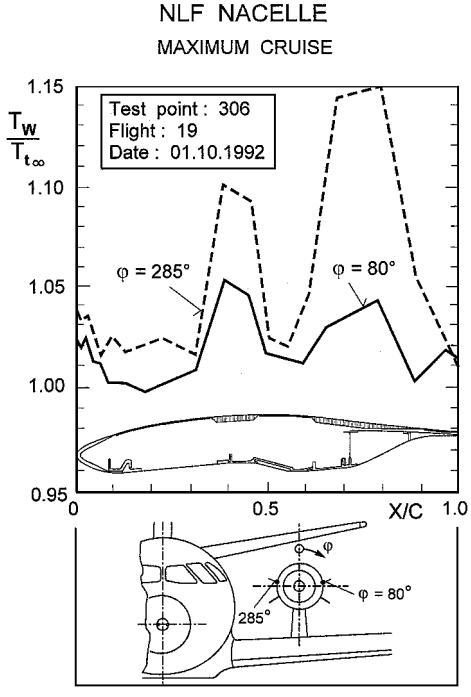

Fig. 10 NLF nacelle fan cowl external surface temperature distributions for the maximum cruise condition, showing the effect of incorrect wall temperature sensor installation (TP 306).

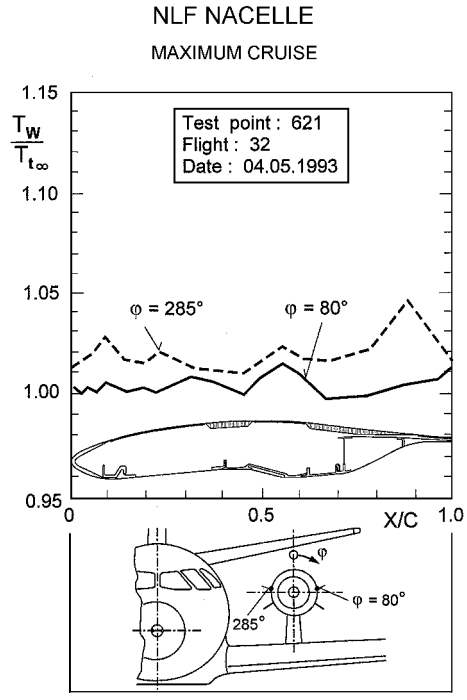

Fig. 11 NLF nacelle fan cowl external surface temperature distributions for the maximum cruise condition, showing the improvement achieved (TP 621) after relocation of the wall temperature sensors.

of TP 306. However, there exists a considerable waviness in the temperature distributions, which makes the detection of the transition location not an easy task.

What kind of surface temperature distribution was actually expected will be demonstrated with reference to results obtained flight testing the HLF nacelle. The fan cowl of this nacelle featured, to the rear of the suction zone, a uniform honeycomb substructure extending longitudinally nearly right up to the fan cowl trailing edge (Fig. 4). This particular structural layout of the fan cowl was a result of previous experience gained from the flight trials with the NLF and Datum nacelles. Figure 12 shows, for the HLF nacelle fan cowl, the surface temperature distribution at radial $\varphi = 84$ deg and Fig. 13 the thermogram of the outboard fan cowl for the cruise condition with suction applied. The results refer to TP 821 obtained in the third flight series; details of the associated flight conditions are listed in Table 1. The surface temperature distributions at $\varphi = 84$ deg exhibits the expected trend with a higher temperature level in the laminar flow region on the fan cowl than for the turbulent flow. Temperature resolution is of such quality that the onset of transition ($x_{\mathrm{Tro}}/c = 0.55$) and that of the fully turbulent flow ($x_{\mathrm{Tfo}}/c = 0.65$) can be clearly identified. Noting that the CFC material of the fan cowl is a poor heat conductor, the transition length of $(x_{\mathrm{Tfo}}/c - x_{\mathrm{Tro}}/c) = 0.10$ can be expected to be a good approximation of the actual transition length. The location of the transition front, defined by the midpoint T_r between x_{Tro}/c and x_{Tfo}/c, is at $x/c = 0.60$, which agrees well with the transition front position at $\varphi = 84$ deg on the thermogram.

For a closer examination of the temperature distributions on the NLF nacelle fan cowl at $\varphi = 80$ deg for the maximum cruise condition (TP 621), this is replotted on a larger ordinate scale in Fig. 14. To facilitate the detection of the transition location from the surface temperature distributions, Fig. 15 shows the associated thermogram. In addition, surface static pressure distributions for the upper ($\varphi = 30$ deg) as well as the lower ($\varphi = 140$ deg) outboard quadrants of the NLF nacelle fan cowl are presented in Fig. 14. The surface static pressure distributions supplement the infrared thermographic technique concerning the transition detection in the following way. As a rule-of-thumb method, which is applicable to aerodynamically clean surfaces and Reynolds numbers in the range from $Re_c = 5 \times 10^6$ to 10×10^6, the trend of the distribution of the

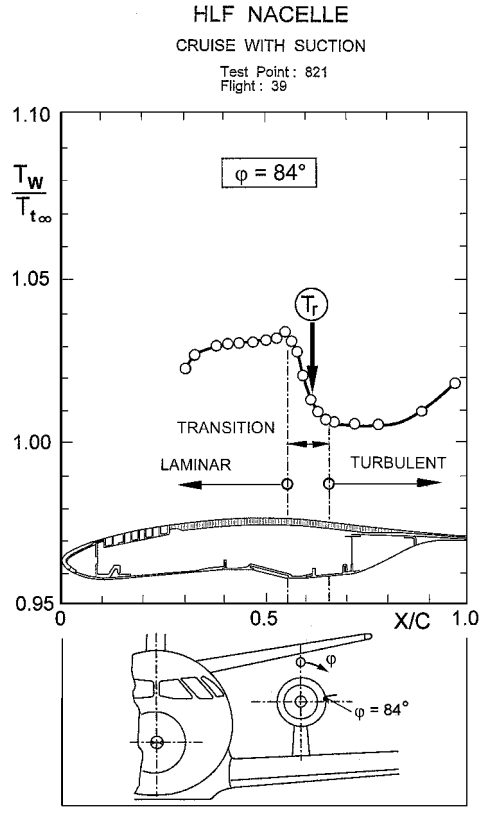

Fig. 12 HLF nacelle fan cowl external surface temperature distribution for the cruise condition with suction (TP 821), with T_r indicating the flow transition location.

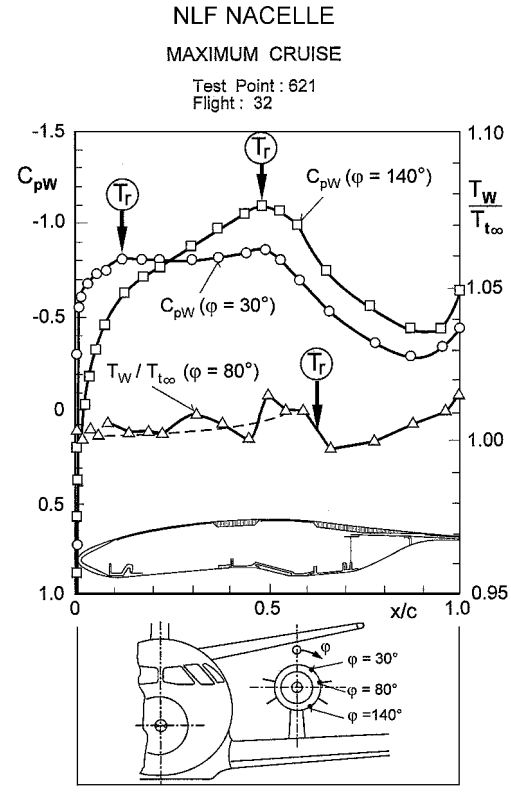

Fig. 14 NLF nacelle outboard fan cowl external surface static pressure and temperature distributions for the maximum cruise condition (TP 621), with T_r indicating the respective flow transition locations.

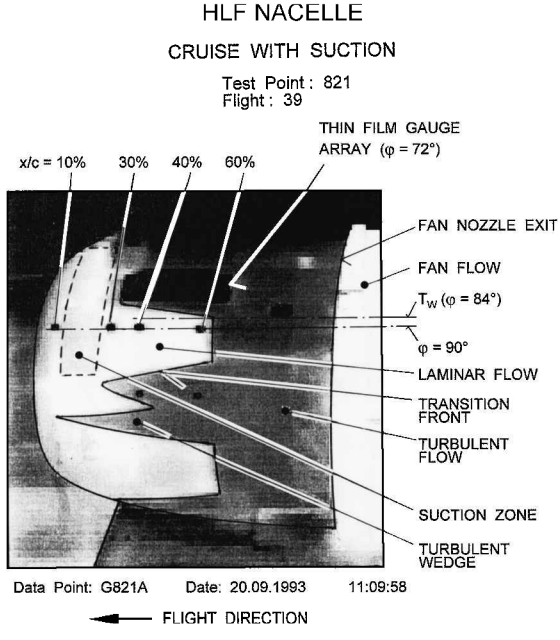

Fig. 13 Infrared image of the outboard fan cowl of the HLF nacelle for the cruise condition with suction (TP 821).

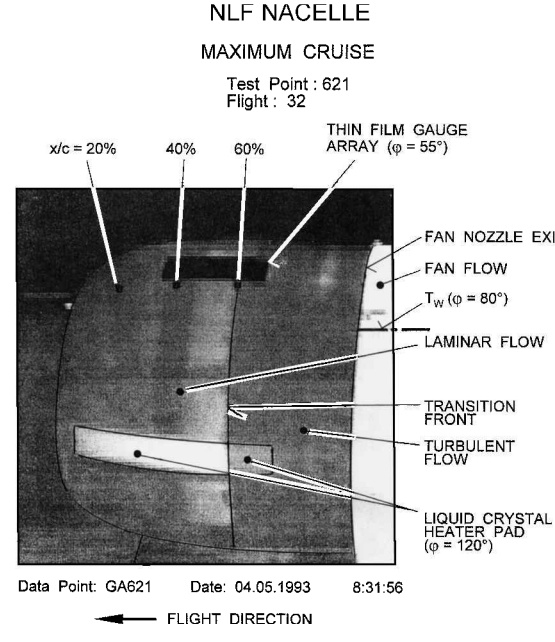

Fig. 15 Infrared image of the outboard fan cowl of the NLF nacelle for the maximum cruise condition (TP 621).

surface static pressure coefficient C_{PW} acts as guide in the sense that a favorable pressure gradient, that is, streamwise decreasing values of the static pressure coefficient, can be taken as an indication for the existence of a laminar boundary layer on the fan cowl.[4] Thus, under these conditions, laminar boundary-layer flow will exist with certainty for a run from the stagnation point up to the first suction peak. In Fig. 14, these peaks, and with them the transition locations, are indicated by T_r. The position of the flow transition determined in this way is conservative. When the thermogram and the surface static pressure distributions C_{PW} are used as background information regarding the location of the transition front and when that section of the surface temperature distribution $T_w/T_{t\infty}$ for which waviness exists is smoothed by a mean line (dashed line in Fig. 14), it is possible to determine the transition location from the respective surface temperature distribution on this basis. In Fig. 14, the dashed line representing the mean temperature distribution at $\varphi = 80$ deg on the outboard fan cowl ends at $x/c = 0.60$, with T_r marking the position of the transition. This is confirmed by comparison with the

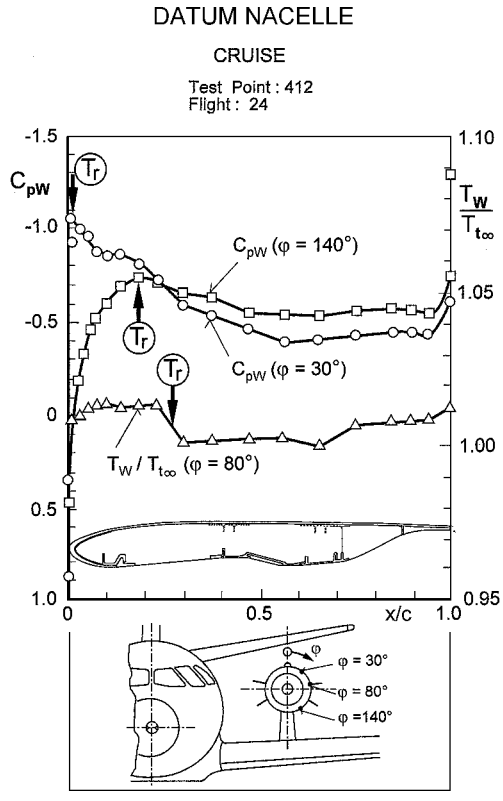

Fig. 16 Datum nacelle outboard fan cowl external surface static pressure and temperature distributions for the cruise condition (TP 412), with T_r indicating the respective flow transition locations.

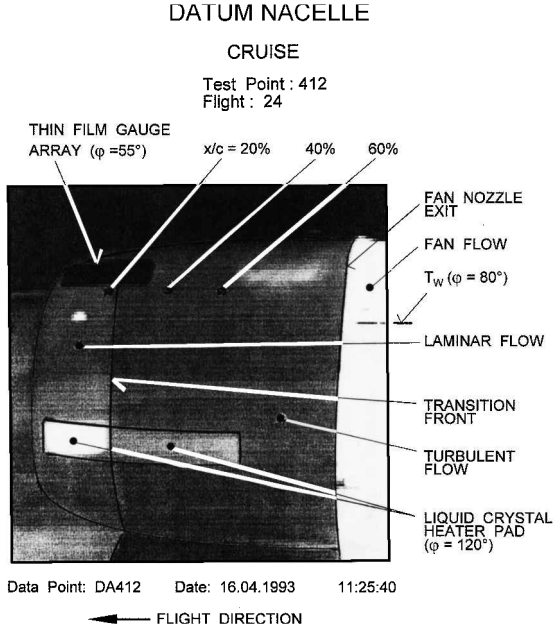

Fig. 17 Infrared image of the outboard fan cowl of the Datum nacelle for the cruise condition (TP 421).

location of the transition front on the associated thermogram, noting that there is electric heating of the liquid crystal heater pad.

The Datum nacelle fan cowl features a CFC skin structure that is nearly uniform over the entire chord length excluding the bird-strike glass-fiber layup in the region of the highlight (Fig. 4). Figure 16 illustrates, for the cruise condition (TP 412, Table 1), the surface temperature distribution $T_w / T_{t\infty}$ at $\varphi = 80$ deg for the outboard fan cowl. In contrast to the situation encountered for the surface temperature distribution on the NLF nacelle fan cowl, it is found that for the Datum nacelle fan cowl the surface temperature distribution exhibits hardly any waviness so that the transition location T_r is readily determined at $x/c = 0.25$ for $\varphi = 80$ deg. From the trend of the surface static pressure distribution at $\varphi = 30$ and 140 deg with the conservative estimate of the transition position T_r, there is supporting evidence that the transition location at $\varphi = 80$ deg lies at $x/c = 0.25$. Final evidence for this is contained in the thermogram of Fig. 17, which shows a situation where the liquid crystal heater pad at $\varphi = 120$ deg is subjected to electric heating.

Conclusions

Several boundary-layer flow transition detection methods have been applied in the course of flight-testing CFC conventional and laminar flow nacelles on the DLR flight-test vehicle VFW614/ATTAS. The flight trials were conducted within the framework of a European collaborative program to investigate an NLF and an HLF nacelle in comparison with a Datum (conventional) nacelle. The flow transition detection methods comprised infrared thermography and surface temperature measurements, as well as the use of thin-film gauges and liquid crystal heater pads. In the present study, attention has been focused mainly on the influence of environmental phenomena and of the powerplant structure regarding the interpretation of the nacelle fan cowl infrared images and of the fan cowl surface temperature measurements. The study has yielded the following results.

1) The quality of the infrared images is influenced by heat radiation to space and from the Earth.

2) The infrared image quality also essentially depends on the position of the nacelle relative to the sun, as well as on the reflection of the sunlight from the airframe (wing and fuselage).

3) To facilitate flow transition detection, only CFCs should be used as structural material for the nacelle fan cowls. This also applies to the suction chambers and the substructure (inner skin) of the insect anticontamination zone in the case of the HLF nacelle.

4) For the transition detection using infrared thermography, it is required that the mechanical design of the fan cowl should not contain any stiffening frames but should aim at a uniform honeycomb skin structure.

5) For good quality fan cowl surface temperature measurements, a uniform honeycomb CFC skin structure is just as essential as for the infrared imaging system.

6) To not impair the quality of the fan cowl surface temperature measurements, careful mounting of the surface temperature sensors directly underneath the final coating of paint on the fan cowl is essential.

7) No premature transition has been observed on any of the fan cowls flight tested from pressure tappings tripping the laminar boundary-layer flow. The tappings had a nominal tap diameter of 0.20 –0.30 mm. The flight trials covered Reynolds numbers up to $Re_c = 9.6 \times 10^6$, a maximum Mach number of $M_\infty = 0.60$, and altitudes up to $H \approx 7{,}620$ m.

8) The infrared imaging system yielded the flow transition front as a well-defined line. A transition length, that is, a boundary-layer run for which the flow changed from the transition onset to fully turbulent flow, was not identifiable.

9) Surface temperature distributions on a CFC skin with honeycomb substructure, exemplified by the HLF nacelle fan cowl, allowed a transition length and the position of the transition front to be determined. The transition length observed can be expected to be a good approximation of the actual transition length due to the poor heat conductivity of the CFC skin.

References

[1] Shipley, P. P., Birch, N. T., Riedel, H., Horstmann, K. H., and Lücking, P. A., "A European Collaborative NLF Nacelle Flight Demonstrator," *Proceedings of the 1st European Forum on Laminar Flow Technology*, Congress Centrum, Hamburg, Federal Republic of Germany, Paper 92-01-005, March 1992.

[2] Barry, B., Parke, S. J., Bown, N. W., Riedel, H., and Sitzmann, M., "The Flight Testing of Natural and Hybrid Laminar Flow Nacelles," International

Gas Turbine and Aeroengine Congress and Exposition of the American Society of Mechanical Engineers, ASME Paper 94-GT-408, June 1994.

[3]Mullender, A. J., and Riedel, H., "A Laminar Flow Nacelle Flight Test Programme," Abstracts 2nd European Forum on Laminar Flow Technology, Association Aéronautique et Astronautique de France, Paper 2.4, June 1996.

[4]Riedel, H., Horstmann, K. H., Ronzheimer, A., and Sitzmann, M., "Aerodynamic Design of a Natural Laminar Flow Nacelle and the Design Validation by Flight Testing," *Aerospace Science and Technology*, Vol. 2, No. 1, 1998, pp. 1–12.

[5]Riedel, H., and Sitzmann, M., "Some Aspects of Flow Transition Detection when Flight Testing Carbon Fibre Composite Conventional and Laminar Flow Nacelles," DLR, German Aerospace Research Center, Rept. DLR-Forschungsbericht 1999-37, Brunswick, Germany, 1999.

[6]Horstmann, K. H., Redeker, G., Quast, A., Dreßler, U., and Bieler, H., "Flight Tests with a Natural Laminar Flow Glove on a Transport Aircraft," AIAA 8th Applied Aerodynamics Conf. 1990: A Collection of Technical Papers, Portland, Oregon, Pt. 1, CP907, AIAA, Washington, DC, Aug. 1990, pp. 385–392.

[7]Gartenberg, E., and Roberts A. S., Jr., "Twenty-Five Years of Aerodynamic Research with Infrared Imaging," *Journal of Aircraft*, Vol. 29, No. 2, 1992, pp. 161–171.

[8]Quast, A., "Detection of Transition by Infrared Image Technique," *International Congress on Instrumentation in Aerospace Facilities* (ICIASF'87 Record), Inst. of Electrical and Electronics Engineers, New York, 1987, pp. 125–134.

[9]Quast, A., "Bestimmung des laminar-turbulenten Umschlags mit Hilfe der Infrarottechnik," Rept. IB 129-86/6, DFVLR, Brunswick, Germany, Oct. 1997.